16th World Conference on Earthquake Engineering, 16WCEE 2017

Santiago Chile, January 9th to 13th 2017

Paper N° 2004 (Abstract ID)

Registration Code: S-T1464737601

Development of Offshore Probabilistic Tsunami Exceedance Amplitudes for ASCE 7-16

H.K. Thio[1], Y. Wei[2], G. Chock[3], W. Li[4]

[1] *Principal Seismologist, AECOM Los Angeles, CA, USA, hong.kie.thio@aecom.com*
[2] *Research Scientist, University of Washington, Seattle, Washington, USA, yong.wei@noaa.gov*
[3] *President, Martin & Chock, Inc., Honolulu, Hawaii, USA*
[4] *Coastal Engineer, AECOM, Los Angeles*

…

Abstract

We have developed probabilistic tsunami offshore amplitude exceedance maps, with an average return period of 2500 yr, for the five Pacific states of the USA to be used as basis for the tsunami design guidelines of ASCE 7-16. These maps are based on a comprehensive integration over tsunamigenic earthquakes on all the circum-Pacific subduction zones. Thanks to the linear behavior of tsunami waves in the deep ocean, we are able to use an efficient Green's function summation approach to model, which enabled us to integrate over thousands of events. An integral part of the analysis is the formal inclusion of epistemic uncertainties, resulting from a limited understanding of the physical processes as well their aleatory variability due to the randomness in natural processes.

We can divide the offshore tsunami hazard problem into two stages: the source characterization and deep ocean propagation. In the source characterization, many of the epistemic uncertainties and aleatory variabilities are identical to those specified in probabilistic seismic hazard analysis (PSHA). The biggest difference is in the details of slip distributions, which are very significant in tsunami excitation, especially for near-field tsunamis, but are not used in PSHA. We have used a simplified asperity model to include this variability.

These offshore hazard maps are used to anchor the tsunami inundation zones included in ASCE 7-16, developed by NOAA, and are also used as a constraint for site-specific inundation studies as prescribed in the standards.

Keywords: *tsunami; hazard; probabilistic;*

1 Introduction

The upcoming revision of ASCE 7-16 ("Minimum Design Loads and Associated Criteria for Buildings and Other Structures"), which forms the basis of building codes in the USA, will for the first time include a chapter on tsunami loads. As with other natural hazards, the design parameters are location dependent and maps of design values are included in the chapter. In this paper we describe the process for obtaining the offshore probabilistic exceedance amplitudes for the five states bordering the Pacific Ocean. This map, to be included in the ASCE 7-16 document, forms the basis of the maps of the tsunami inundation zones [1] as well as site-specific procedures for inundation outlined in the chapter.

2 Background

Although tsunami hazard at return periods of engineering interest is dominated by those caused by earthquakes, there are some marked differences between the probabilistic tsunami hazard analysis (PTHA) and its seismic equivalent probabilistic seismic hazard analysis (PSHA). It is helpful for understanding our approach to list some of the characteristics of tsunami waves:

1. Frequency of occurrence – over the last hundred years, there have been on average 10 documented tsunami events per year worldwide, three per year causing waveheights exceeding 1 m (Table 1) and only one per year causing at least one fatality. Tsunamis are therefore relatively rare events and for any one location the historical record is far too short for a meaningful statistical analysis. Instead, we have to rely on judgment to a large degree.
2. Far-field effects – There have been many occurrences of tsunamis causing damage and fatalities over very large distances (thousands of kilometers): e.g. 1946 Alaska earthquake in Hawai'i, 1964 Alaska earthquake in Crescent City and Hawai'i, 2004 Sumatra event in Sri Lanka, India and East Africa. Tsunamis travelling across the deep ocean basins have negligible energy loss through attenuation. Furthermore, the very long wavelengths associated with megathrust earthquakes have very little dispersion, and the linearity of the wavefront emanating from a predominantly line source reduces the effect of geometrical spreading in the direction perpendicular to the orientation of the line-source.
3. Strong directivity – tsunami sources introduce a strong directionality (Fig. 1). For earthquakes, this is a function of the dip of the fault and the rake of the slip vector. Usually, the maximum of the tsunami radiation pattern coincides with the orientation of the least geometrical spreading, so these effects reinforce each other. In the case of submarine landslides we find very strong directivity in the sliding direction.
4. Strong influence from sea floor topography and coastal geometry – the bathymetry of the oceans varies greatly. Even in the open ocean, topographical features such as plateaus and especially ridges and seamount chains strongly influence the propagation characteristics (Fig. 1). For instance, submarine ridges have a lower propagation velocity compared to the surrounding basin and will therefore act as a waveguide, focusing waves in the direction of the ridge [2]. In the nearshore regime, the shape of the shoreline can lead to focusing and de-focusing of waves and also to resonances, which can locally amplify the waves significantly [3].
5. No saturation at large magnitudes – contrary to seismic hazard, tsunami amplitudes do not reach some saturation level for very large magnitudes. The hazard analysis is therefore sensitive to the maximum magnitude of the source models

Based on the above characteristic and other features, it is clear that a fully empirical hazard analysis is not feasible. Over the last few decades however, numerical modeling techniques and increased computational power combined with improvements in the accuracy and resolution of bathymetrical models have allowed us to model tsunami with a great degree of precision. Currently, computing high-resolution inundation models are still expensive in terms of CPU time, so that in order to perform a fully probabilistic analysis we need to reduce the event integration to a manageable subset. We have solved this problem by using a two-stage approach, consisting of a fully probabilistic offshore hazard mapping followed by higher-resolution inundation mapping anchored by the offshore probabilistic amplitudes. In this paper we describe the first stage of the mapping that was carried out for the ASCE 7-16 tsunami design maps. The second stage inundation mapping will be described in a companion paper [1].

Table 1 – Tsunamis over the last 100 yr

Fatalities	0	≥ 1	≥ 10	≥ 100	≥ 1,000	≥ 10,000	≥ 100,000
1916-2016	943	116	69	39	16	3	1
Max. runup	>0 m	>1 m	>2 m	>5 m	>10 m	> 20 m	> 50 m
1916-2016	1059	316	232	133	73	29	11

3 Probabilistic offshore wave amplitude hazard

3.1 Overview

The methodology behind PSHA is well known (e.g., [4]) and here we will only briefly describe the adaptations that are made for PTHA. Whereas in PSHA we are usually interested in the exceedance of some ground motion measure such as peak ground acceleration (PGA) or spectral acceleration (SA), in PTHA a parameter of interest (not necessarily the only one) is the maximum tsunami height that is expected to be exceeded at sites along the coast. The earthquake recurrence models behind the two methods are the same. The difference lies in the process that relates the occurrence of an earthquake with certain magnitude and location to the hazard at the site, such as the Ground Motion Prediction Equations (GMPE) in PSHA. In the empirically derived GMPE, this relationship is a simple function of magnitude and distance, with some corrections applied for source and site characteristics. Because of the aforementioned strong laterally varying nature of tsunami propagation, we have adopted a waveform excitation and propagation approach instead of trying to develop analogous tsunami prediction equations. In fact, current developments in PSHA include the replacement of the GMPE's with ensembles of numerically generated ground motions, which is analogous to the approach proposed here ([5]).

The excitation and propagation of tsunamis in deeper water can be modeled using the shallow water wave approximation, which is linear for amplitudes that are significantly smaller than the water depth ([6]). We can solve the equation of motion numerically using a finite-difference method, which has been validated to produce accurate tsunami heights for propagation through the oceans, although for very shallow water the amplitudes may become too large, and more sophisticated nonlinear methods are required to model the details of the run-up accurately. Nevertheless, the linear approach provides a very good first approximation of tsunami propagation, taking into account the effects of lateral variations in seafloor depth.

3.2 Green's Function Summation

The underlying principle for this approach is the validity of the linear behavior of tsunami waves. This enables us to deconstruct a tsunami that is generated by an earthquake into a sum of individual tsunami waveforms (Green's functions) from a set of subfaults that adequately describe the complexities in earthquake rupture. By pre-computing and storing the tsunami waveforms at points along the coast generated by each subfault for a unit slip, we can efficiently synthesize tsunami waveforms for any slip distribution by summing the individual subfault tsunami waveforms weighted by their slip. The same principle is used in the inversion of tsunami waves for earthquake rupture (e.g., [6]). This efficiency makes it feasible to use Green's function summation in lieu of attenuation relations to provide very accurate estimates of tsunami height for probabilistic calculations, where one typically needs to compute thousands of earthquake scenarios. For instance, once the Green's functions were computed, the probabilistic tsunami amplitude results in this paper for which we integrated over more than 10,000 scenarios, were computed on a single 24-core computer in a few hours.

The assumption of linearity is not valid for tsunamis where the amplitudes are comparable to the water depth. Also, the detailed bathymetry near the shoreline is important to estimate the final run-up heights. Therefore, we have computed the offshore Green's functions at a target depth of 100 m.

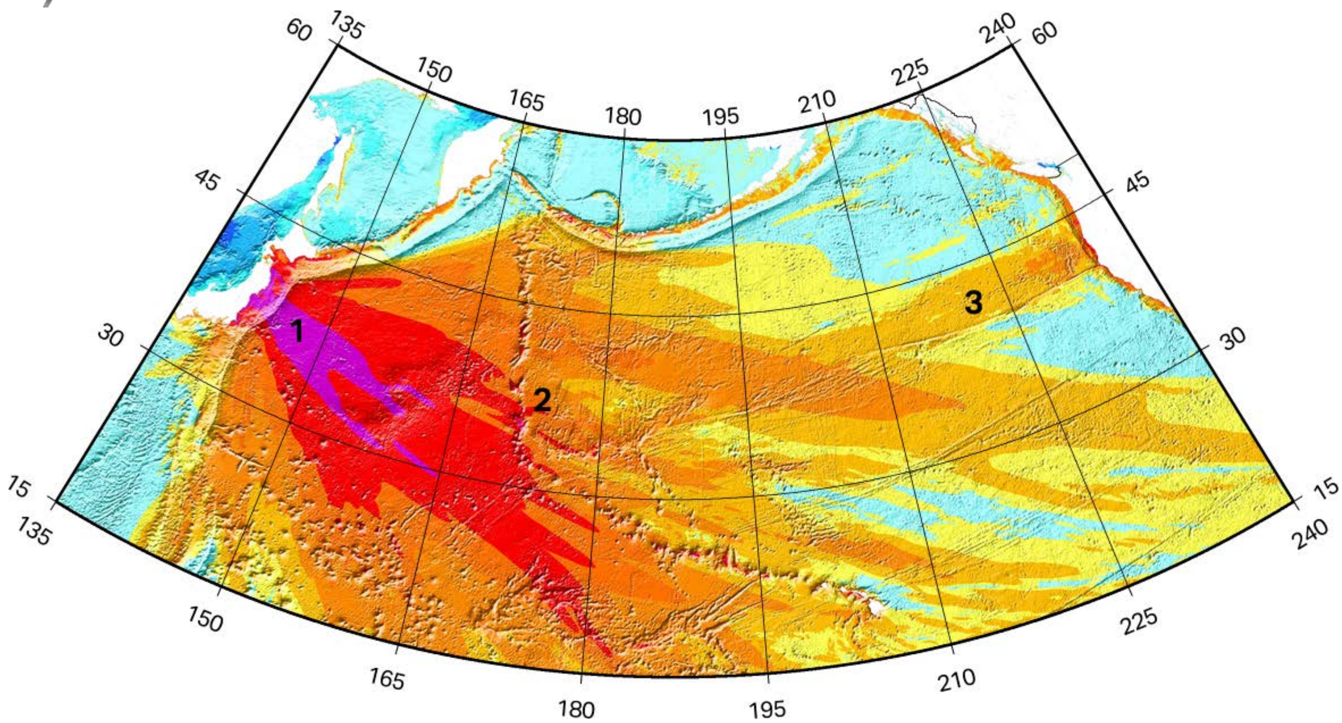

Fig. 1 – Maximum amplitudes for a model of the 2011 Tohoku tsunami. Some typical tsunami characteristics are: 1 – largest amplitudes perpendicular to the strike of the fault rupture, 2 – strong influence of bathymetric features on the propagation and amplitudes, 3 – amplification of waves due to relatively low propagation velocities, e.g. north of the Mendocino fracture zone.

4 Methodology

4.1 Probabilistic analysis

The probabilistic framework that we developed is based on the procedures used in Probabilistic Seismic Hazard Analysis (PSHA), with the fundamental difference over traditional PSHA being the use of modeled hazard parameters (such as wave amplitude) rather than empirically derive ground motion prediction equations.

PSHA is based on methodology originally proposed by Cornell [7] and we will present a brief overview of the method as well as specific information on the parameters and models used in our analysis. Assuming a time-independent (Poissonian) recurrence model, the probability that a hazard, such as PGA in seismic and wave amplitude in PTHA, exceeds a certain value (*s*) in a time period *t* is given by:

$$P(A > s) = 1 - e^{-\phi(s)t} \tag{1}$$

where $\phi(s)$ is the annual mean number of events (also known as "annual frequency of exceedance") in which the hazard parameter of interest exceeds the value *s*. For engineering purposes, we are interested in computing s for a certain probability of occurrence, *P*, in a time period *t*. For this project, the targets are probabilities of 2%, 5%, 10% and 50% occurrence in a time span of 50 years, which is equivalent to annual frequencies of exceedance of 1/2475, 1/975, 1/475 and 1/72 per year respectively. We usually refer to the latter in terms of return period, e.g. 475 and 72 years.

The annual frequency of exceedance is calculated as follows:

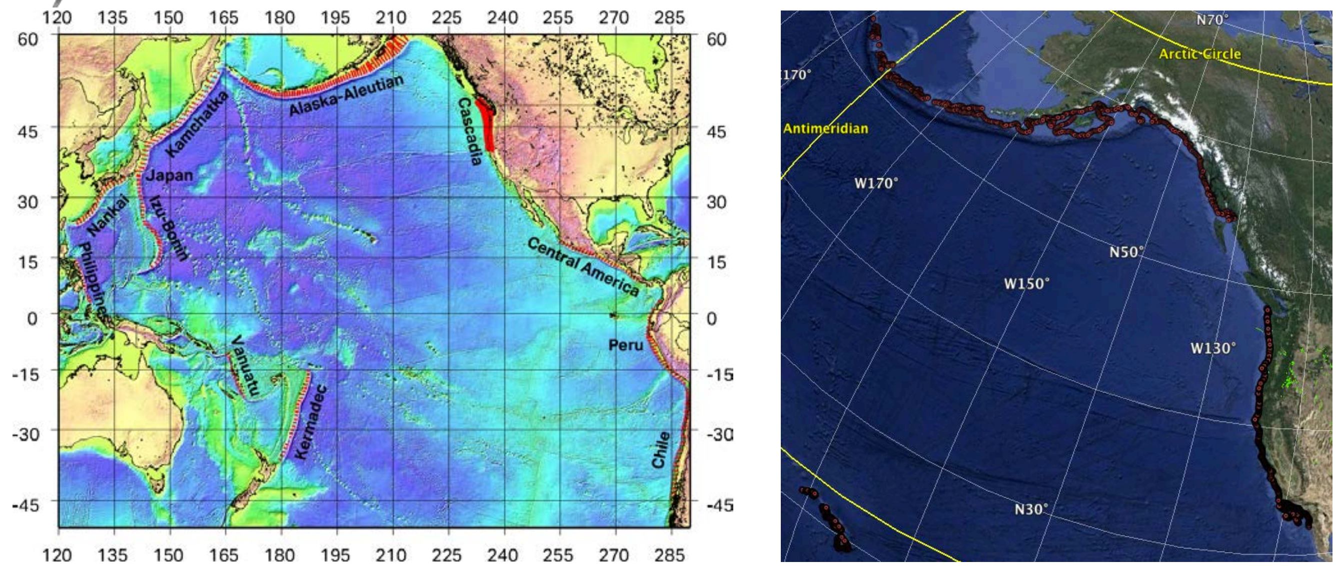

Figure 2. a) (left) map of the Pacific Ocean showing the source locations used in this study. B) (right) – Map showing the western 5 States and the locations of the offshore points considered in the ASCE 7-16 maps.

$$\phi(s) = \sum_{i=1}^{Faults} \left(\iint_{m,r} f(m)(P(A > s \mid m,r)P(r \mid m)\, dm\, dr \right)_i \qquad (2)$$

where:

f(m_i) = probability density function for events of magnitude m_i

P(A>s|m,r) = probability that amplitude *A* exceeds *s* given magnitude *m* and source at *r*

P(r|m) = probability for a source at *r*, given a source of magnitude *m*.

Whereas in traditional PSHA the *r* term represents source to site distance, in our case it refers more generally to the source location *r* with the propagation from the source to the site computed explicitly through the Green's function approach instead of an attenuation relation. Uncertainties associated with seismic source parameters, such as geometry, location, rupture scenario and recurrence rates were incorporated using a logic tree approach.

4.2 Epistemic uncertainties

Uncertainties due to an incomplete understanding of natural processes, which require us to use judgment to quantify, are called epistemic uncertainties, and the way these uncertainties are incorporated is fundamentally different than the way aleatory uncertainties are included. In our analysis, the following uncertainties are deemed epistemic:

- Fault segmentation (single or multi-segment ruptures)
- Slip rate (actual slip rate or fraction of slip seismogenic slip rate)
- Recurrence model

In principal, the epistemic uncertainties should only include those parameters for which a subjective judgment is made, and different logic tree branches represent different understanding of the same process. For instance, a large fault may have ruptured along different segments in the past, and some may argue that this segmentation represents a fundamental property of the fault and therefore only segmented ruptures are allowed. Others might argue that there is no compelling reason why the fault cannot rupture in multi-segment ruptures, and in their opinion multi-segment ruptures are allowed. In such case, we can define (at least) two weighted logic tree branches whose weights are chosen to represent the likelihood that a branch represents the correct behavior of the fault, with the weights adding up to one.

In practice, the distinction between epistemic and aleatory uncertainties is not always clear, and for convenience' sake aleatory uncertainties are sometimes incorporated through logic tree branches, i.e. as epistemic uncertainties. This usually does not affect the mean hazard, but it will affect fractile results.

4.3 Logic Trees

The discrete nature of the epistemic uncertainties is expressed through the use of logic trees, where all the different manifestations of a process are represented as a branch of a logic tree.

Uncertainties in the model parameters are generally incorporated using a logic-tree approach, where different alternatives are represented as weighted branches. These include variations in slip-rate, magnitude range and distribution, fault geometry, as well as rake. As already mentioned, dip variations would normally also be considered under the epistemic uncertainties, but because these would require a new set of Green's functions, we have added them as an aleatory uncertainty.

In the Green's function approach, it is convenient to divide these uncertainties into two groups: parameter variations that act on the Green's function level (e.g., fault geometry) and parameters that do not influence the Green's functions, such as the recurrence parameters and magnitude scaling relations. In the latter case, the logic tree branches are easily added without major computational requirements, but for the former, the question is whether any extra branch in the logic tree, such as a variation in slip, would require an entire set of Green's functions. From some simple numerical experiments, we conclude that in many cases, especially at large distances, these variations can accurately be taken into account by perturbing the Green's functions using a constant scaling factor rather than re-computing them. For example, a change in rake, readily translates into a change of the vertical seafloor displacement, which in turn directly translate to differences in waveheight.

At shorter distances, i.e., local faults, this approach is less accurate, and in these situations (particularly for dip-slip events) we will have to resort to complete re-computation of the Green's functions. However, since these sources are relatively scarce, and require less computing time due to the short distances, this is far less of a burden than having to re-compute tele-tsunami Green's functions.

4.4 Aleatory variability

Aleatory variability, in a strict sense, reflects the inability to predict the outcome of a process due to its random nature. Whether or not variability in the outcome of a process is truly aleatory, i.e., caused by the random behavior of nature rather than a limited understanding of the process itself, is not always clear, and can even differ from one researcher to the other. Aleatory variability is typically accounted for by the use of distribution functions rather than single mean or median values to express the outcome of a process. The probability of an outcome being in a certain range is then given by the area under the probability distribution function, in most cases normal or lognormal. In our analysis we have identified several significant contributions to the aleatory variability such as magnitude scaling, slip distribution, modeling error and tide stage.

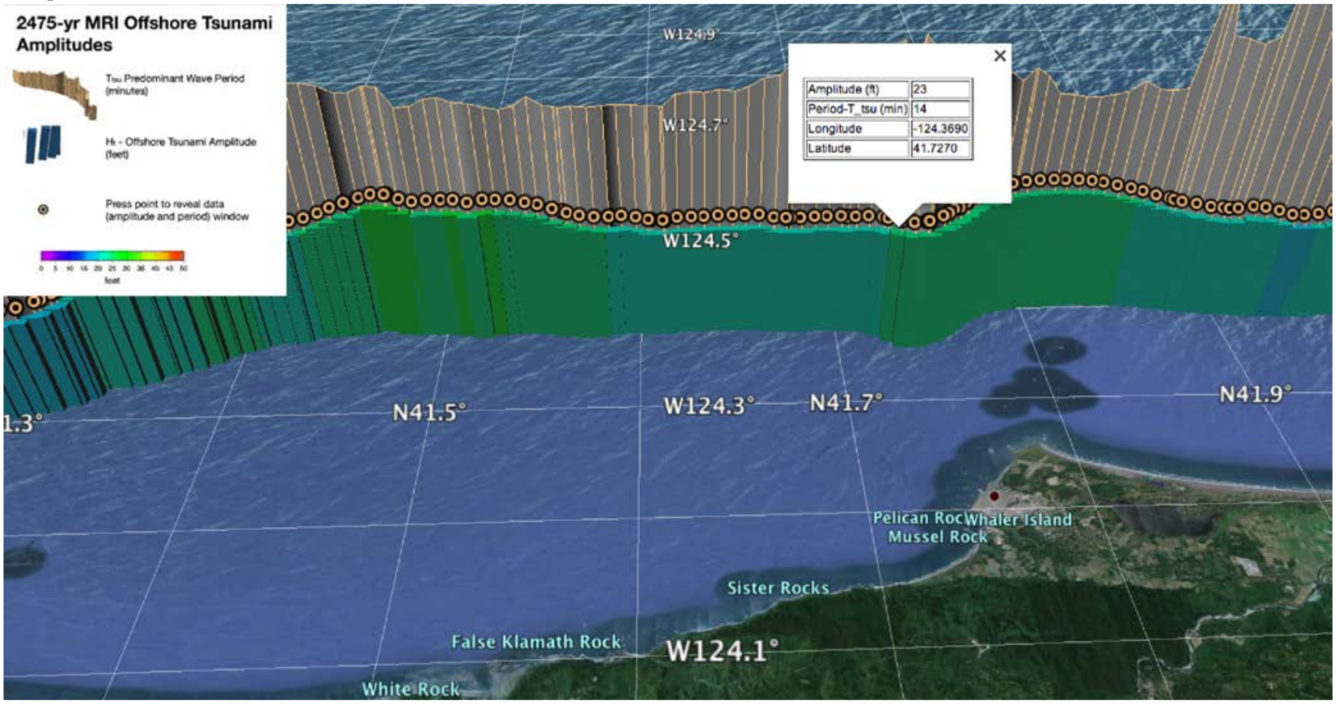

Figure 3. Example of the offshore exceedance amplitudes for north California. The colored bars indicate the amplitudes, whereas the grey fencing represents the dominant wave period. The same information is also interactively visible for each point along the 100 m bathymetric contour as shown in the white box.

4.4.1 Magnitude/average slip

The rupture length (from the base models) and rupture width (from the logic tree) provide us with an area (*A*) which through the published scaling relations, e.g. [8]:

$$M = 4.441 - 0.041 \times \log(A),\ \sigma = 0.286$$

gives us magnitude (*M*), and thus earthquake moment (M_0 – in Nm):

$$M_W = \frac{\log(M_0) - 9.1}{1.5}$$

The average slip is (*D*) then obtained through:

$$D = \frac{M_0}{\mu A}$$

We sample the magnitude area distribution at five points from -2 to +2 sigma.

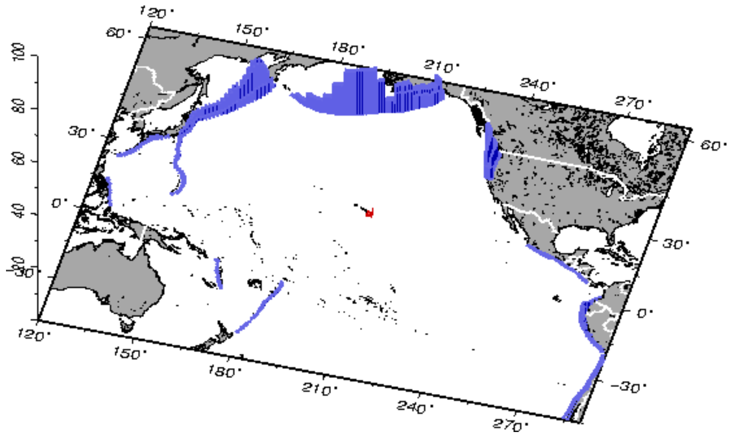

Figure 4. Source disaggregation for a site in Hawai'i and a 2500 yr hazard level. The blue bars express the relative contribution of a particular fault element to the hazard.

4.4.2 Variable slip

In previous analyses (e.g. [9,10]), we have used uniform slip models to produce tsunami waves. At local distances however, the slip variability becomes an important factor and asperities with large amounts of slip can cause significantly higher tsunami waves, especially locally, as is illustrated by the recent Tohoku earthquake where the maximum slip exceeded the average slip by at least a factor of 2.

Murotani et al. [11] studied the slip distributions of several subduction zone earthquakes and found a ratio of maximum slip over average slip of 2.2. To include this slip variability, we used variable slip rupture models with on third of the rupture as an asperity with twice the average slip and the other two-thirds of the rupture at half the average slip. In order to achieve uniform long-term slip we computed a total of three scenarios for each event where the asperity occupies every part of the rupture once. This way, there is no risk that in some areas the hazard is over- or under-estimated due to incomplete or overlapping asperity coverage offshore.

4.4.3 Tidal variability

The tidal variability is included in the offshore waveheights for the tele-tsunami sources by convolving the time-series with a local tidal record. This ensures that in the case of multiple high waves, the probability of coinciding with a high tide is properly taken into account. For the Cascadia source, our original intent was to compute scenarios at a number of tide levels, and weigh them according to a similar distribution function. However, that would increase the number of runs dramatically and we decided instead to include the tidal component for the local runs in the same way as the aleatory uncertainty for the inundation, i.e. after the inundation has been computed.

4.4.4 Tsunami modeling error

Thio et al. [11] included a sigma term for the modeling uncertainty based on the analysis of observed and modeled tsunami waveheights for several well-constrained tsunamis along the west coast. These uncertainties only cover the oceanic propagation to the shoreline since most data were obtained from tide gage records. For the aleatory uncertainty in the inundation and runup from a local earthquake we need to establish a new term, which requires detailed modeling of runup data from a well-constrained event. The recent Tohoku earthquake provides a wealth of data for this purpose, and we have used this event to determine a sigma term for the tsunami model.

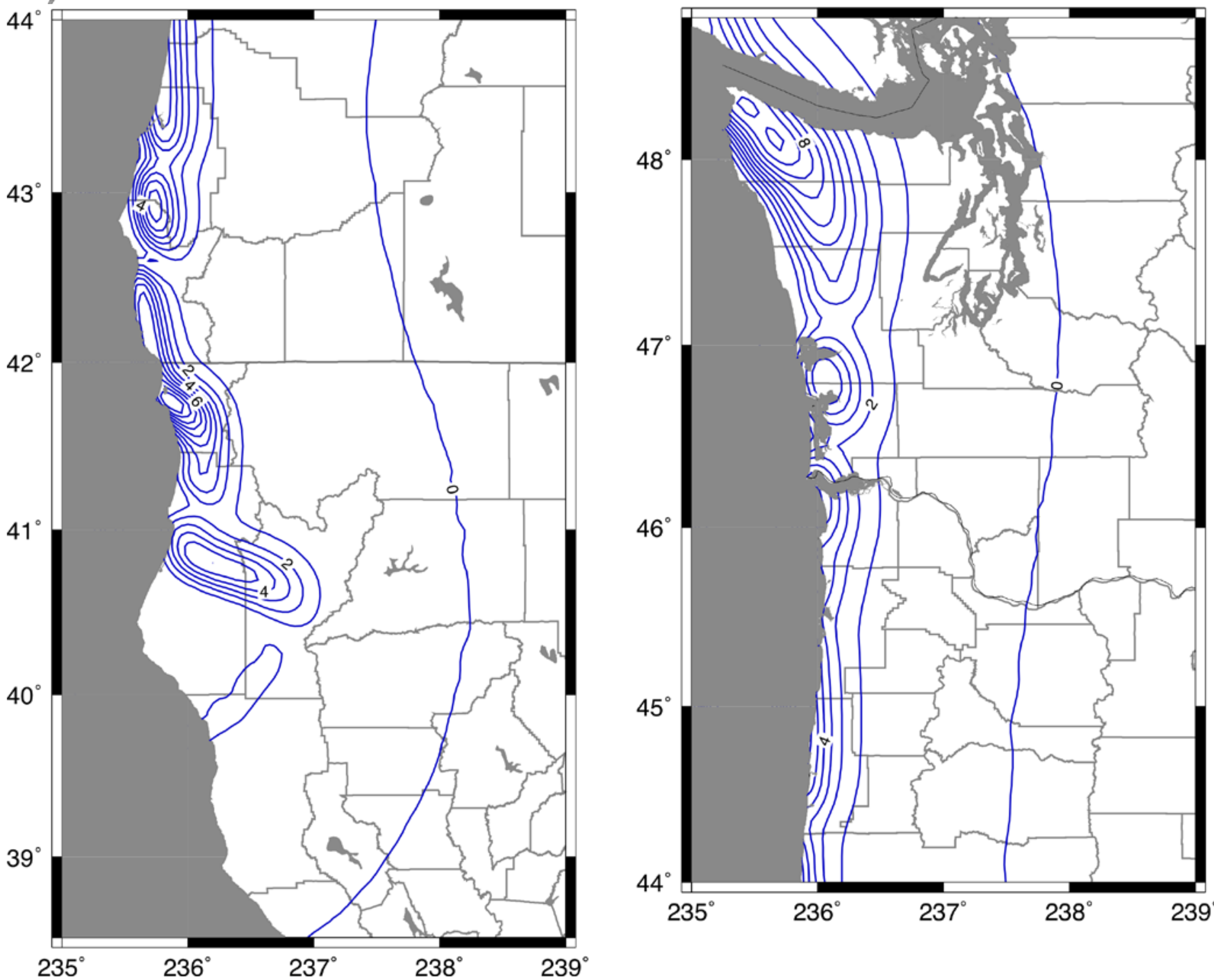

Fig. 5. Probabilistic (2500 yr return period) subsidence contours (in feet) for the Cascadia coast. These maps are based on the same set of events that was used for the offshore PTHA.

5 Sources

5.1 Distant sources

We have included megathrust sources from around the Pacific (Fig. 2a). Except for Cascadia and Alaska, the recurrence models are based on simple relations between maximum magnitudes and fault dimensions as well as global convergence rates. To express different tectonic environments, we did use seismic coupling coefficients. The Cascadia model is based on the recent update to the national seismic hazard maps [12] but for Alaska we used a more extensive logic tree since a lot of recent data has emerged (e.g. [13]), which was not part of the earlier USGS seismic model [14]. Since both the Cascadia and Alaska-Aleutian sources are within the target areas for the tsunami hazard, we took particular care in both the resolution of the fault geometry (based on 1x1 km fault elements) but also on the distributed slip variability.

6 Results

In Fig. 3 we present an example of the 2500 yr offshore exceedance amplitude and dominant period in northern California (Crescent City). The colored bars are exceedance amplitudes at the 100m depth contour, and then beige fencing shows the dominant wave period. Users can interactively access the actual tables with the values list, as shown in the figure. The map covers the entire coastlines of California, Oregon Washington, Hawai'i and Alaska. They are used as target amplitudes for the development of the tsunami inundation zones [1] but can also be used for site-specific tsunami inundation studies under ASCE 7-16, where the requirement is that the 100 offshore amplitudes are within at least 80% of these offshore maps. For both cases, we also developed source disaggregation maps (Fig. 4) that identify the dominant sources that affect a particular site.

In the case of Alaska and Cascadia, where the subduction zones are located in the target areas, it is also necessary to take into account the co-seismic subsidence hazard, which can be quite substantial in some localities. For this purpose, ASCE 7-16 also includes probabilistic subsidence hazard maps (Fig. 5) for all affected areas. These maps are based on the same event integration used for the tsunami hazard.

7 References

[1] Wei, Y., H. K. Thio, V. Titov, G. Chock, H. Zhou, L. Tan, and C. Moore, (2016). Inundation Modeling To Create 2,500-Year Return Period Tsunami Design Zone Maps For The ASCE 7-16 Standard , Proceedings of the 16th World Conference on Earthquake engineering, Santiago, Chile.

[2] Kowalik, Z., Horrillo, J., Knight, W., & Logan, T. (2008). Kuril Islands tsunami of November 2006: 1. Impact at Crescent City by distant scattering. *Journal of Geophysical Research: Oceans*, *113*(C1), C01020. http://doi.org/10.1029/2007JC004402

[3] Horrillo, J., Knight, W., & Kowalik, Z. (2008). Kuril Islands tsunami of November 2006: 2. Impact at Crescent City by local enhancement. *Journal of Geophysical Research: Solid Earth*, *113*(C1), C01021. http://doi.org/10.1029/2007jc004404

[4] McGuire, R.K., (2004). Seismic Hazard and Risk Analysis, EERI Monograph, 221 pp.

[5] Graves, R., Jordan, T.H., Callaghan, S., Deelman, E., Field, E.H., Juve, G., Kesselman, C., Maechling, P., Mehta, G., Milner, K., Okaya, D., Small, P., Vahi, K., (2010) CyberShake: A Physics-Based Seismic Hazard Model for Southern California. *Pure and Applied Geophysics*, *168*, 367–381.

[6] Satake, K. (1995). Linear and nonlinear computations of the 1992 Nicaragua earthquake tsunami. *Pure and Applied Geophysics*, *144*(3), 455–470.

[7] Cornell, C. A. (1968). Engineering seismic risk analysis. *Bulletin of the Seismological Society of America*, *58*(5), 1583–1606.

[8] Strasser, F. O., Arango, M. C., & Bommer, J. J. (2010). Scaling of the Source Dimensions of Interface and Intraslab Subduction-zone Earthquakes with Moment Magnitude. *Seismological Research Letters*, *81*(6), 941–950. http://doi.org/10.1785/gssrl.81.6.941

[9] Horspool, N., Pranantyo, I., Griffin, J., Latief, H., Natawidjaja, D.H., Kongko, W., Cipta, A., Bustaman, B., Anugrah, S.D., and Thio, H.K. (2014) A probabilistic tsunami hazard assessment for Indonesia. *Natural Hazards and Earth System Sciences*, *14*, 3105–3122.

[10] Thio, H. K., Somerville, P. G., & Polet, J. (2016). Probabilistic Tsunami Hazard Analysis (pp. 1–9). Presented at the 15th World Conference on Earthqake Engineering.

[11] Murotani, S., Satake, K., & Fujii, Y. (2013). Scaling relations of seismic moment, rupture area, average slip, and asperity size for M~9 subduction-zone earthquakes. *Geophysical Research Letters*, *40*(19), 5070–5074. http://doi.org/10.1002/grl.50976

[12] Petersen, M.D., Moschetti, M.P., Powers, P.M., Mueller, C.S., Haller, K.M., Frankel, A.D., Zeng, Yuehua, Rezaeian, Sanaz, Harmsen, S.C., Boyd, O.S., Field, Ned, Chen, Rui, Rukstales, K.S., Luco, Nico, Wheeler, R.L., Williams, R.A., and Olsen, A.H., 2014, Documentation for the 2014 update of the United States national seismic hazard maps: U.S. Geological Survey Open-File Report 2014–1091, 243 p., *http://dx.doi.org/10.3133/ofr20141091*.

[13] Witter, R. C., Briggs, R. W., Engelhart, S. E., Gelfenbaum, G., Koehler, R. D., & Barnhart, W. D. (2014). Little late Holocene strain accumulation and release on the Aleutian megathrust below the Shumagin Islands, Alaska. *Geophysical Research Letters*, *41*(7), 2359–2367. http://doi.org/10.1002/(ISSN)1944-8007

[14] Wesson, Robert L., Boyd, Oliver S., Mueller, Charles S., Bufe, Charles G., Frankel, Arthur D., Petersen, Mark D., 2007, Revision of time-Independent probabilistic seismic hazard maps for Alaska: U.S. Geological Survey Open-File Report 2007-1043.